Supporting Information

Self-Generated Nanoporous Silver Framework for High-Performance Iron Oxide Pseudocapacitor Anodes

*Jae Young Seok, Jaehak Lee, and Minyang Yang**

Department of Mechanical Engineering, Korea Advanced Institute of Science and Technology(KAIST), 291 Daehak-ro, Yuseong-gu, Daejeon 305-701, Republic of Korea

*Corresponding author, E-mail: myyang@kaist.ac.kr

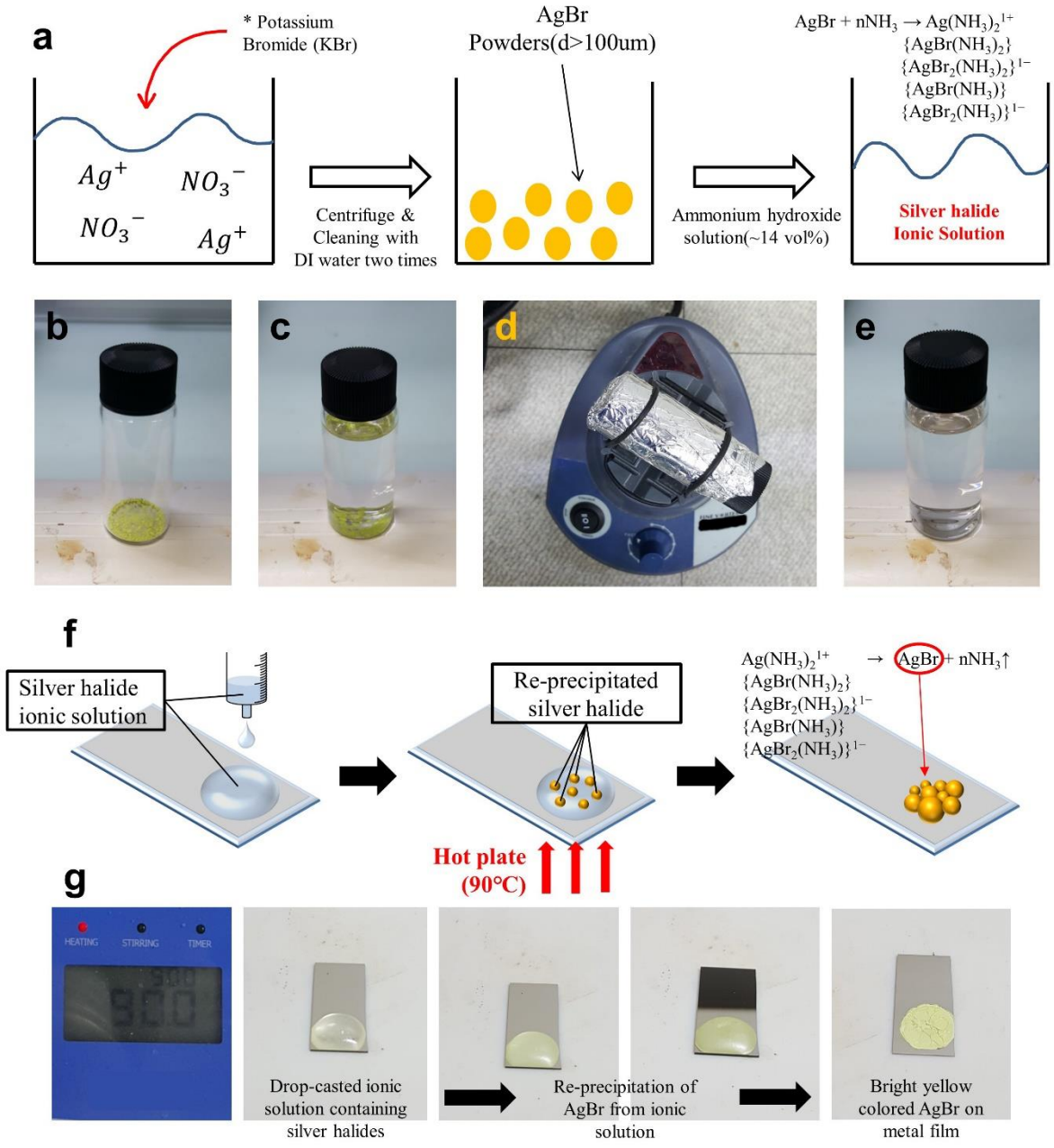

Figure S1. Experimental procedure for fabricating (a) a silver halide ion precursor solution and (b-e) its corresponding digital images. Schematic procedure for (f) deposition of silver halide by drop-casting of the precursor solution, and (g) its corresponding digital images.

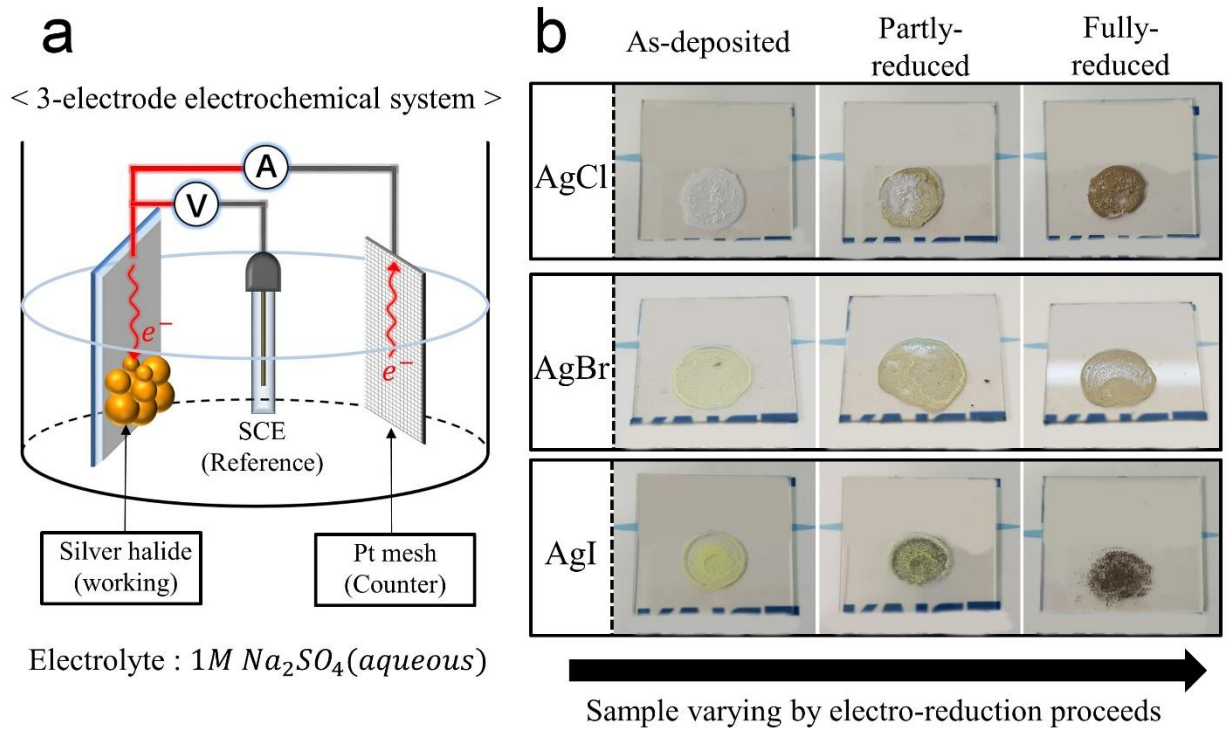

Figure S2. (a) Standard three-electrode electrochemical system composed of a saturated calomel electrode (SCE) as a reference and Pt mesh as a counter electrode. (b) Array of digital images of experimental samples for AgCl, AgBr, and AgI, in the as-deposited, partly reduced, and fully reduced states.

As a representative sample, the bright yellow AgBr particles changed to a brown-colored silver because the unique nanostructure affects the visible wavelength optical absorption properties.

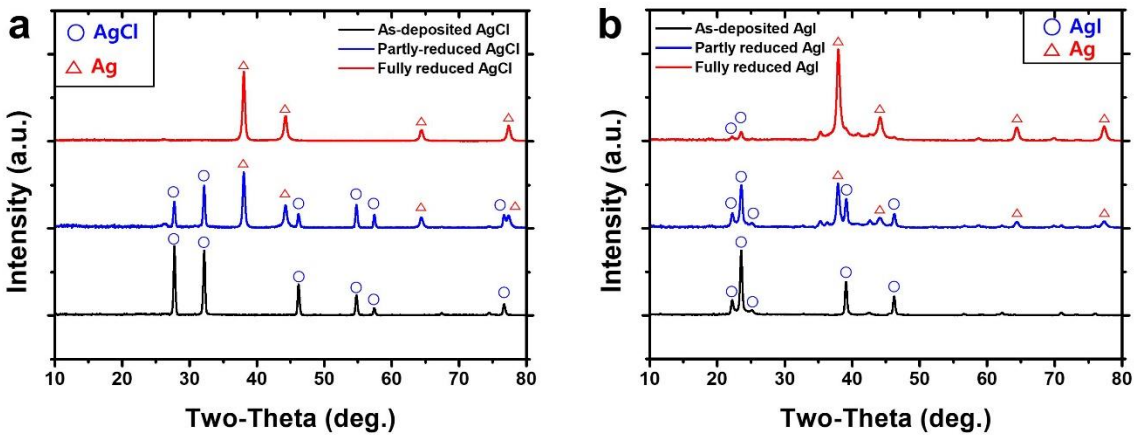

Figure S3. XRD results for the as-deposited state (black line), partly reduced state (blue line), and fully reduced state (red line) for the (a) AgCl and (b) AgI samples.

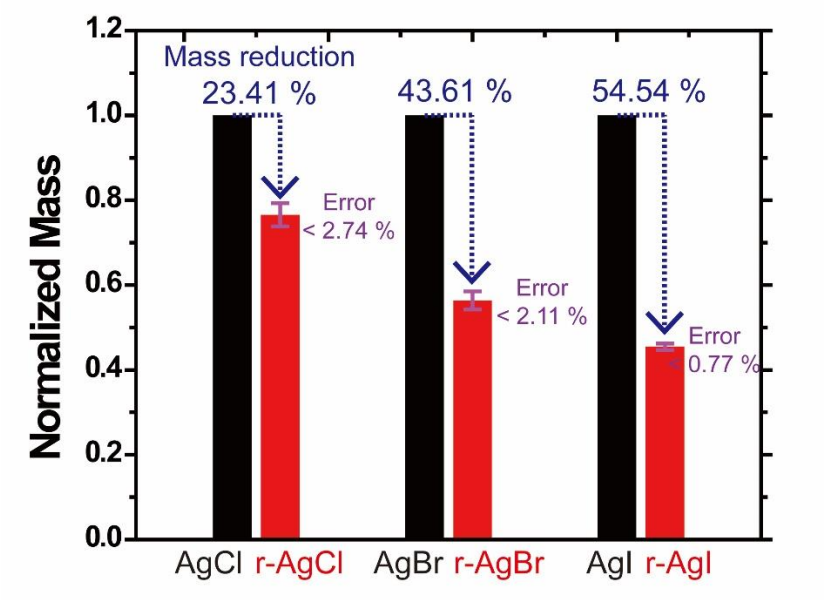

Figure S4. Mass variation ratio between the as-deposited state and fully reduced state of each AgCl, AgBr, and AgI samples.

The mass variation between as-deposited AgX and fully reduced AgX, and the mass decreasing rate (%) of each AgX sample is shown in the bar graph. When AgCl, AgBr, and AgI are reduced to pure Ag, the mass decreasing rates are stoichiometrically 25.4%, 43.1%, and 54.5%, respectively. The mass variation for the AgCl, AgBr, and AgI samples are 23.5%, 43.7%, and 54.5%, respectively, which is assumed to be identical to the stoichiometric values by considering the slight experimental error.

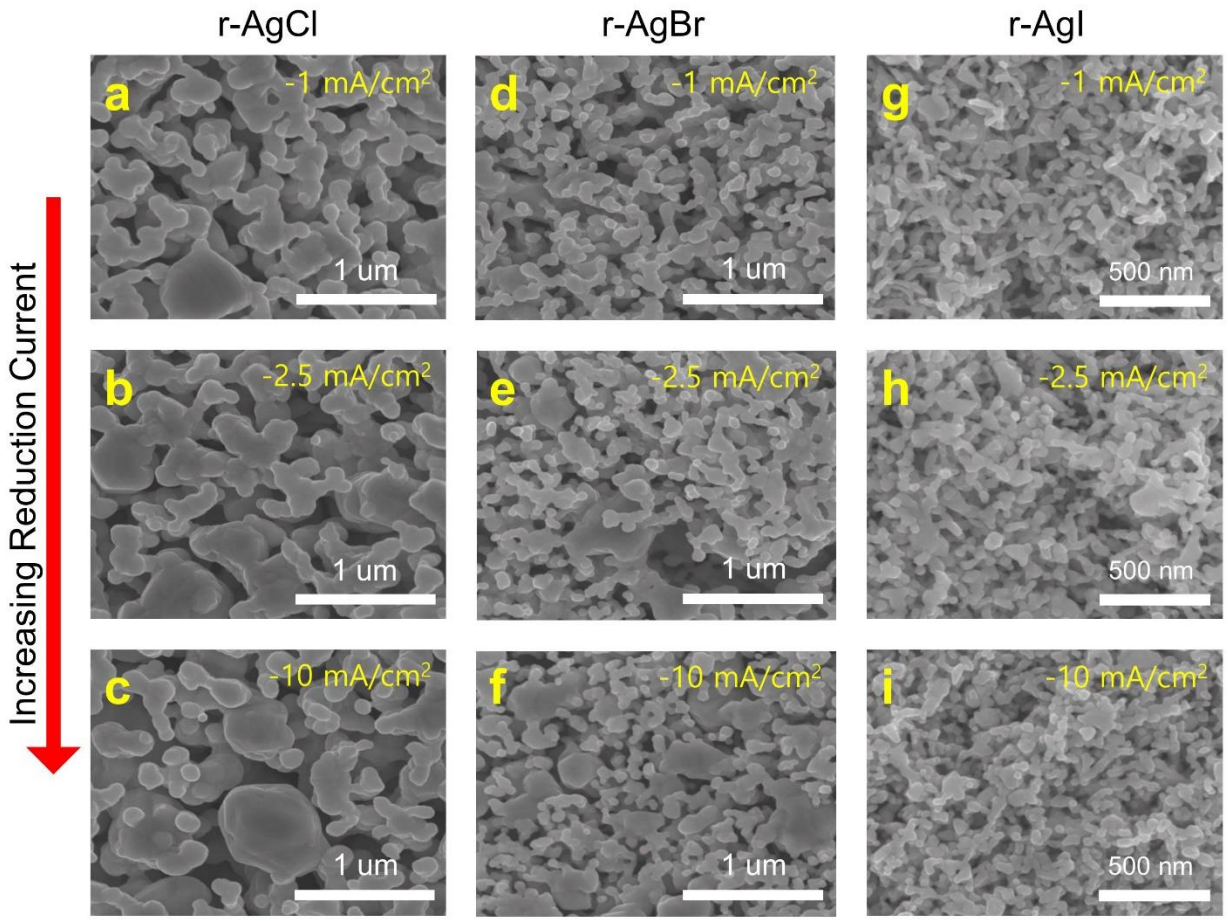

Figure S5. Structural formation with respect to the reduction current during the silver halide electroreduction process. High-magnification SEM images of (a-c) reduced AgCl, (d-f) reduced AgBr, and (g-i) reduced AgI with increasing reduction currents.

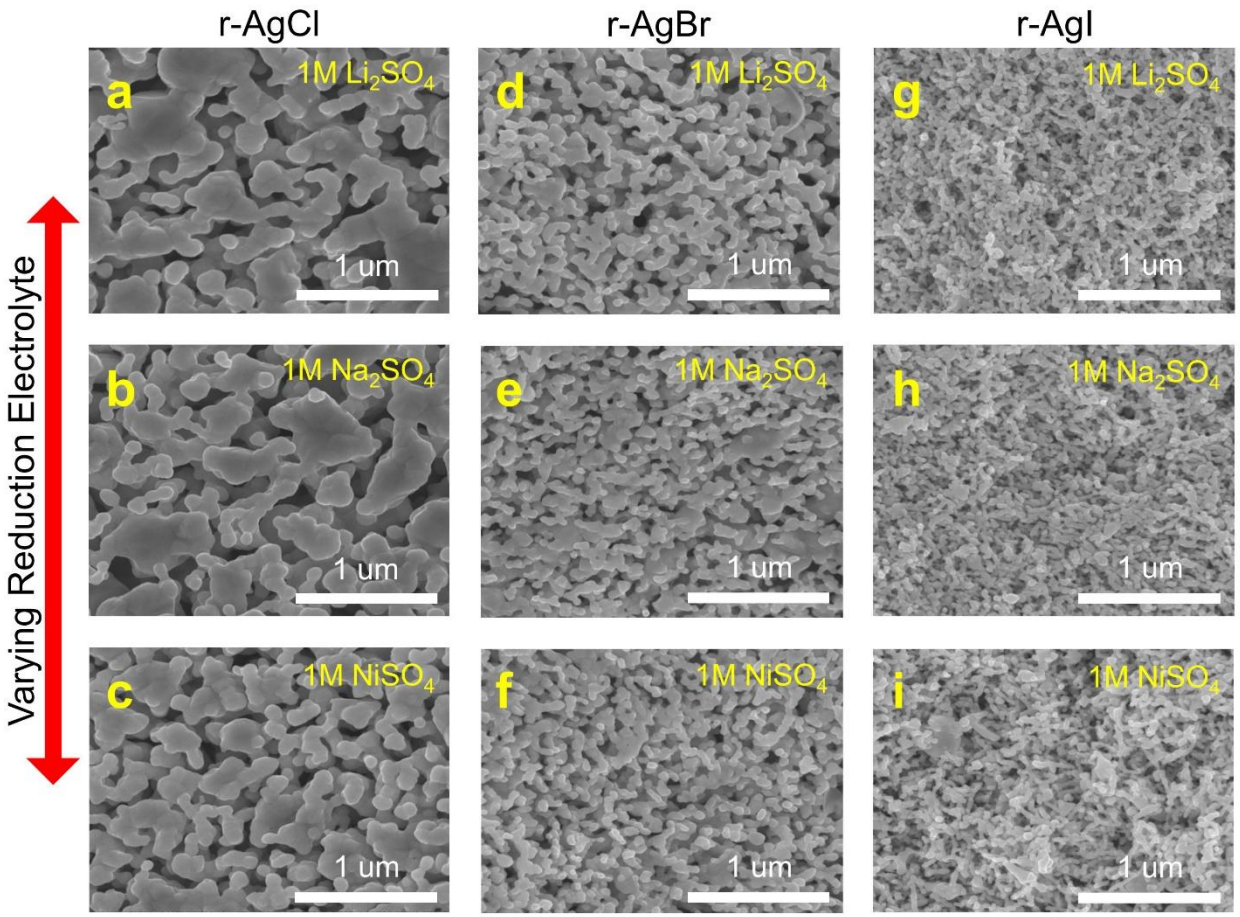

Figure S6. Structural formation differences caused by different reduction electrolytes during the silver halide electroreduction process. High-magnification SEM images of (a-c) reduced AgCl, (d-f) reduced AgBr, and (g-i) reduced AgI using different reduction electrolytes.

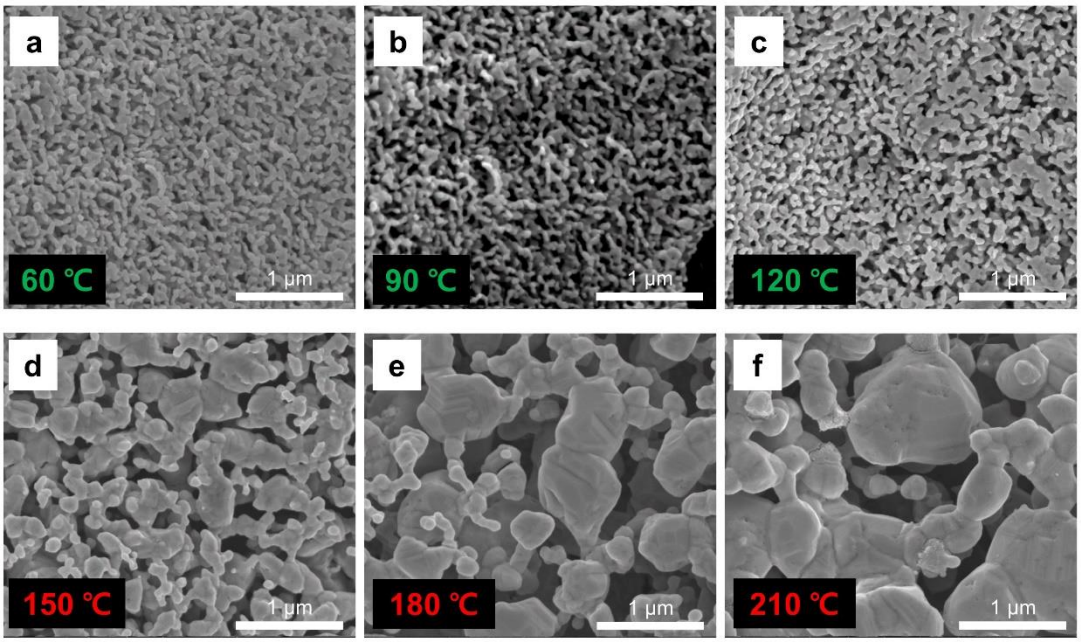

Figure S7. SEM images of the np-Ag framework to confirm thermal stability of np-Ag. Each sample was heat treated at (a) 60 ℃, (b) 90 ℃, (c) 120 ℃, (d) 150 ℃, (e) 180 ℃ and (f) 210 ℃ for 1 hour.

SEM images of the np-Ag sample heat-treated for 1 hour at each temperature are shown in Figure S7. The np-Ag framework is stable up to 120 ℃, however above 150 ℃, the np-Ag framework begins to aggregate with each other, forming a thicker, larger ligament structure. This tendency to agglomerate becomes more apparent when the heat treatment temperature is higher.

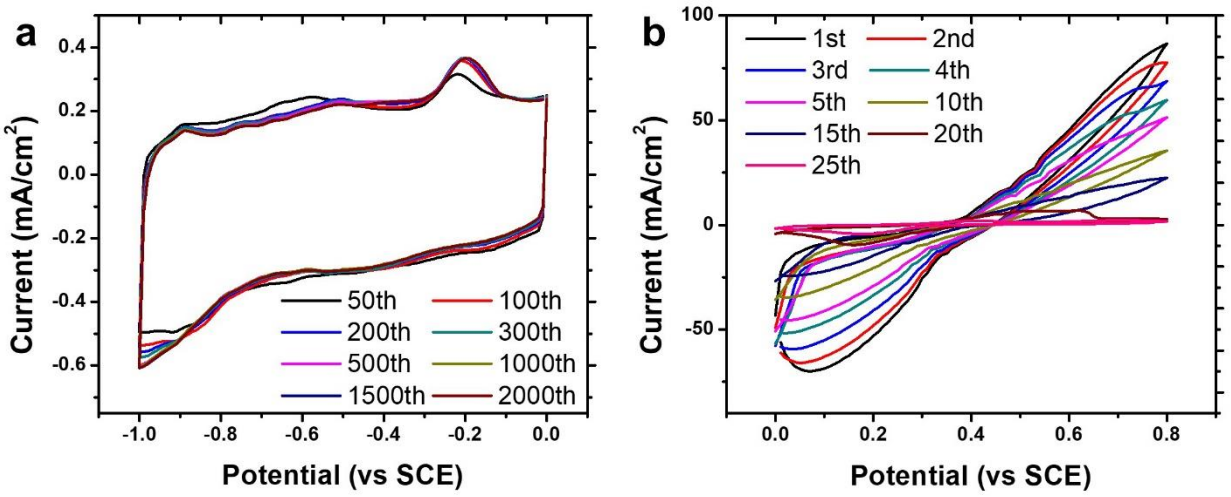

Figure S8. Cyclic voltammetry results of np-Ag framework to confirm electrochemical stability. Voltage window: (a) -1 – 0V, (b) 0 – 0.8V (vs. SCE).

Cyclic voltammetry results of np-Ag framework for each voltage window are shown in Figure S8. Here, the experimental configuration was as follows; SCE was used as a reference electrode, and a platinum foil was used as a counter electrode in a 2.5 M Li_2SO_4 aqueous electrolyte. The np-Ag framework was very stable when the (-) potential was applied and the shape of the CV curve highly stable for over 2000 cycles (Figure S8a). On the other hand, the np-Ag framework degraded sharply when the (+) potential was applied above 0.6 V (Figure S8b). Since the oxidation potential of silver (Ag) is + 0.555 V (vs. SCE), silver was oxidized or dissolved in the electrolyte in the form of Ag^+. As a consequence, this np-Ag framework can be utilized with high stability as an anode material, but it can hardly be applied to a cathode material.

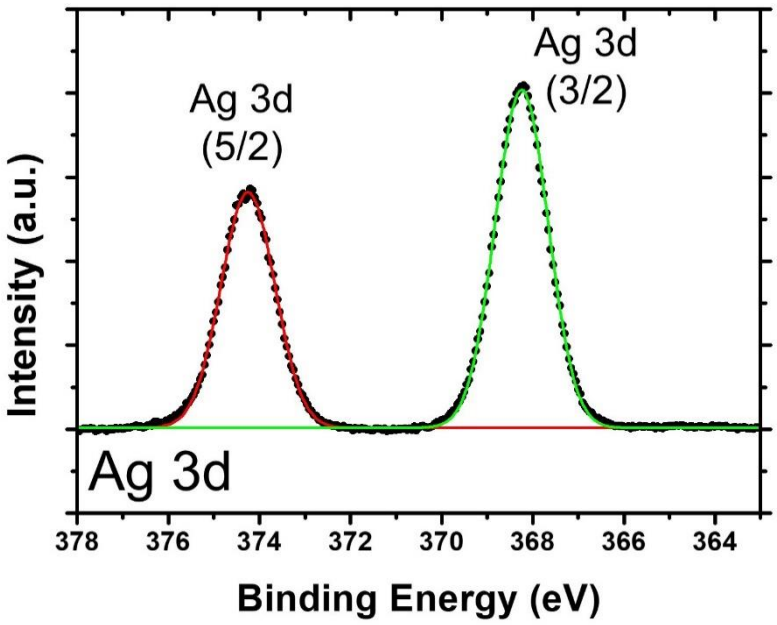

Figure S9. XPS spectrum of Ag 3d for the np-Ag@Fe_2O_3 anode.

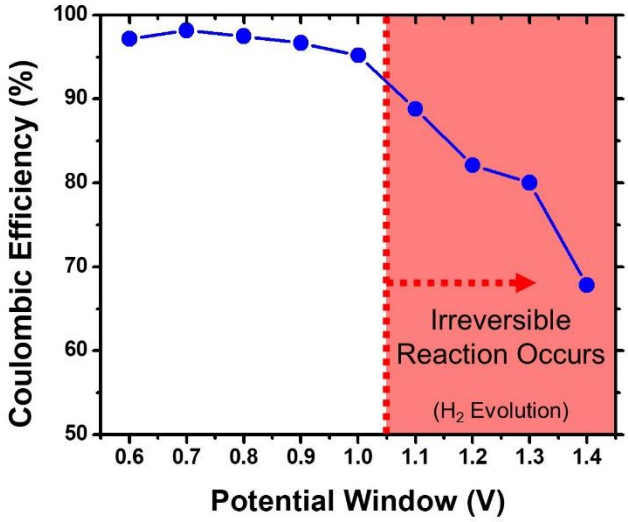

Figure S10. Coulombic efficiencies of np-Ag@Fe_2O_3 electrode during charging/discharging with various potential window.

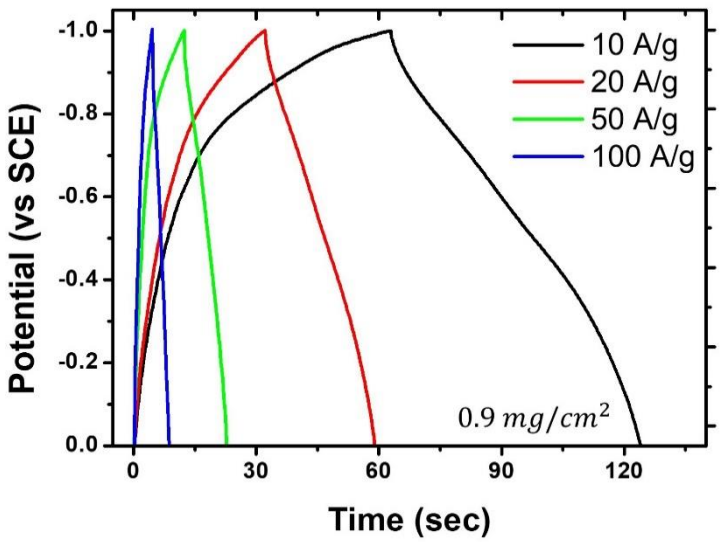

Figure S11. Galvanostatic charge-discharge curves of np-Ag@Fe_2O_3 (with a mass loading of 0.9 mg cm^{-2}) for each charging current density.

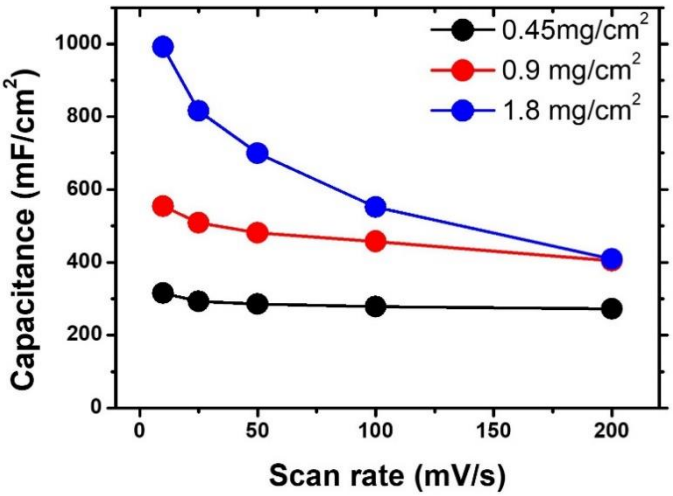

Figure S12. Rate capabilities of np-Ag@Fe_2O_3 by varying the active material mass loading in terms of the areal specific capacitance.

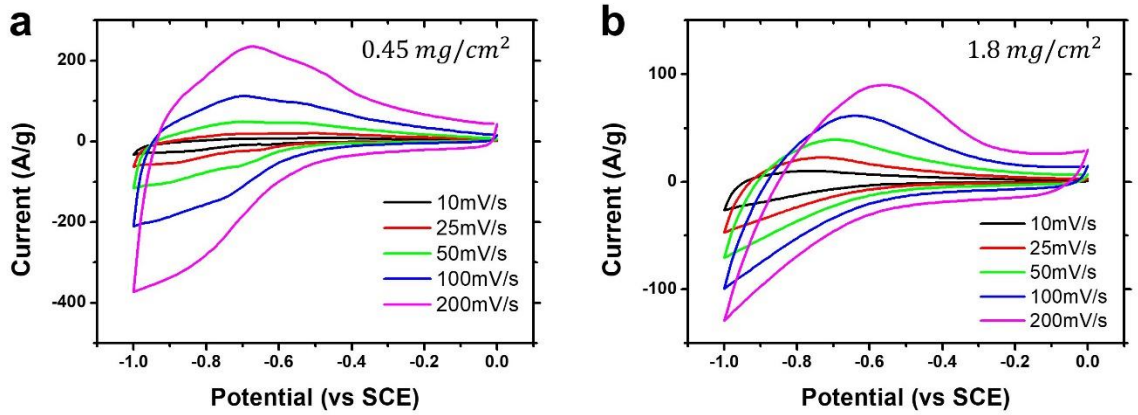

Figure S13. CV curves of the np-Ag@Fe_2O_3 anodes at mass loadings of (a) 0.45 mg cm^{-2} and (b) 1.8 mg cm^{-2}.

Table S1. Comparison of the major figures of merit for np-Ag@Fe_2O_3 using previously reported iron oxide-based (FeO_x-based) electrochemical electrodes with respect to the specific capacitance and cycling performance.

Electrode Structure	Electrolyte	Capacitance	Cyclic stability	Publication Year	Ref
Fe_2O_3 films	0.25 M Na_2SO_4	210 F g^{-1} @ 2 mV s^{-1}	~68.4% after 100 cycles	2006	[1]
Carbon Nanofoam@FeO_x	2.5 M Li_2SO_4	84 F g^{-1} @ 5 mV s^{-1}	~80% after 1000 cycles	2010	[2]
CNT@Fe_3O_4	1 M Na_2SO_4	165 F g^{-1} @ 2 A g^{-1}	~85.1% after 1000 cycles	2011	[3]
rGO@Fe_2O_3 nanotube	1 M Na_2SO_4	215 F g^{-1} @ 2.5 mV s^{-1}	~90% after 2000 cycles	2012	[4]

Carbon nanosheet@Fe_3O_4	1 M Na_2SO_4	163.4 F g^{-1} @ 1 A g^{-1}	~93% after 5000 cycles	2013	[5]
Carbon-coated Fe_3O_4 (core-shell)	1 M Na_2SO_4	275.9 F g^{-1} @ 0.5 A g^{-1}	~81.2% after 500 cycles	2013	[6]
N-doped graphene@Fe_2O_3	1 M Na_2SO_4	260.1 F g^{-1} @ 2 A g^{-1}	~82.5% after 1000 cycles	2014	[7]
Graphene@Fe_2O_3	1 M KOH	908 F g^{-1} @ 2 A g^{-1}	~75% after 200 cycles	2014	[8]
Graphene paper@Fe_3O_4	1 M KOH	368 F g^{-1} @ 1 A g^{-1}	~90% after 1000 cycles	2014	[9]
GF-CNT@Fe_2O_3	2 M KOH	580.6 F g^{-1} @ 5 A g^{-1}	~100% after 50000 cycles	2015	[10]
Graphene aerogel@Fe_2O_3	6 M KOH	393 F g^{-1} @ 1.5 A g^{-1}	~81.5% after 2200 cycles	2016	[11]
Grahene@Fe_2O_3 nanoplate	1 M KOH	510 F g^{-1} @ 5 A g^{-1}	~70% after 1000 cycles	2016	[12]
Hollow carbon@Fe_3O_4	5 M LiCl	193 F g^{-1} @ 1 mV s^{-1}	~94.8% after 10000 cycles	2017	[13]
Nickel Nanotube@Fe_2O_3 Nanoneedles	1 M Na_2SO_4	418.7 F g^{-1} @ 10 mV s^{-1}	~93.3% after 5000 cycles	2017	[14]
Carbon Cloth@FeOOH	2 M KOH	796 F g^{-1} @ 30 A g^{-1}	~91% after 10000 cycles	2017	[15]
Graphene oxide@Fe_2O_3 nanoparticle	3 M KOH	91 F g^{-1} @ 20 mV s^{-1}	Not reported	2017	[16]
Carbon Cloth@Fe_2O_3 Nanorod@Graphene	1 M LiOH	701 F g-1 @ 6 A g-1	~91% after 5000 cycles	2018	[17]
Nanoporous silver@Fe_2O_3	2.5 M Li_2SO_4	616 F g^{-1} @ 10 mV s^{-1} (608 F g^{-1} @ 10 A g^{-1})	~85% after 6000 cycles	This work	-

REFERENCES

[1] Nagarajan, N.; Zhitomirsky, I. Cathodic Electrosynthesis of Iron Oxide Films for Electrochemical Supercapacitors. *J. Appl. Electrochem.* **2006**, *36*, 1399-1405.

[2] Sassin, M. B.; Mansour, A. N.; Pettigrew, K. A.; Rolison, D. R.; Long, J. W. Electroless Depositioni of Conformal Nanoscale Iron Oxide on Carbon Nanoarchitectures for Electrochemical Charge Storage. *ACS Nano* **2010**, *4*, 4505-4514.

[3] Kim, Y. H.; Park, S. J. Roles of Nanosized Fe_3O_4 on Supercapacitive Properties of Carbon Nanotubes. *Current Applied Physics* **2011**, *11*, 462-466.

[4] Lee, K. K.; Deng, S.; Fan, H. M.; Mhaisalkar, S.; Tan, H. R.; Tok, E. S.; Loh, K. P.; Chin, W. S.; Sow, C. H. α–Fe_2O_3 Nanotubes-Reduced Graphene Oxide Composites as Synergistic Electrochemical Capacitor Materials. *Nanoscale* **2012**, *4*, 2958-2961.

[5] Liu, D.; Wang, X.; Wang, X.; Tian, W.; Liu, J.; Zhi, C.; He, D.; Bando, Y.; Golberg, D. Ultrathin Nanoporous Fe_3O_4-Carbon Nanosheets with Enhanced Supercapacitor Performance. *J. Mater. Chem. A* **2013**, *1*, 1952-1955.

[6] Liu, J.; Liu, S.; Zhuang, S.; Wang, X.; Tu, F. Synthesis of Carbon-Coated Fe_3O_4 Nanorods as Electrode Material for Supercapacitor. *Ionics* **2013**, *19*, 1255-1261.

[7] Zhao, P.; Li, W.; Wang, G.; Yu, B.; Li, X.; Bai, J.; Ren, Z. Facile Hydrothermal Fabrication of Nitrogen-Doped Graphene/Fe_2O_3 Composites as High Performance Electrode Materials for Supercapacitor. *J. Alloys Compd.* **2014**, *604*, 87-93.

[8] Wang, H.; Xu, Z.; Yi, H.; Wei, H.; Guo, Z.; Wang, X. One-Step Preparation of Single-Crystalline Fe_2O_3 Particles/Graphene Composite Hydrogels as High Performance Anode Materials for Supercapacitors. *Nano Energy* **2014**, *7*, 86-96.

[9] Liu, M.; Sun, J. In situ Growth of Monodisperse Fe_3O_4 Nanoparticles on Graphene as Flexible Paper for Supercapacitor. *J. Mater. Chem. A* **2014**, *2*, 12068-12074.

[10] Guan, C.; Liu, J.; Wang, Y.; Mao, L.; Fan, Z.; Shen, Z.; Zhang, H.; Wang, J. Iron Oxide-Decorated Carbon for Supercapacitor Anodes with Ultrahigh Energy Density and Outstanding Cycling Stability. *ACS Nano* **2015**, *9*, 5198-5207.

[11] Khattak, A. M.; Yin, H.; Ghazi, Z. A.; Liang, B.; Iqbal, A.; Khan, N. A.; Gao, Y.; Li, L.; Tang, Z. Three Dimensional Iron Oxide/Graphene Aerogel Hybrids as All-Solid-State Flexible Supercapacitor Electrodes. *RSC Adv.* **2016**, *6*, 58994-59000.

[12] Quan, H.; Cheng, B.; Xiao, Y.; Lei, S. One-Pot Synthesis of α-Fe_2O_3 Nanoplates-Reduced Graphene Oxide Composites for Supercapacitor Application. *Chem. Eng. J.* **2016**, *286*, 165-173.

[13] Shi, X.; Zhang, S.; Chen, X.; Tang, T.; Mijowska, E. Effect of Iron Oxide Impregnated in Hollow Carbon Sphere as Symmetric Supercapacitors. *J. Alloys Compd.* **2017**, *726*, 466-473.

[14] Li, Y.; Xu, J.; Feng, T.; Yao, Q.; Xie, J.; Xia, H. Fe_2O_3 Nanoneedles on Ultrafine Nickel Nanotube Arrays as Efficient Anode for High-Performance Asymmetric Supercapacitors. *Adv. Funct. Mater.* **2017**, *27*, 1606728.

[15] Owusu, K. A.; Qu, L.; Li, J.; Wang, Z.; Zhao, K.; Yang, C.; Hercule, K. M.; Lin, C.; Shi, C.; Wei, Q.; Zhou, L.; Mai, L. Low-crystalline iron oxide hydroxide nanoparticle anode for high-performance supercapacitors. *Nat. Commun.* **2017**, *8*, 14264.

[16] Tanaka, S.; Salunkhe, R. R.; Kaneti, Y. V.; Malgras, V.; Alsehri, S. M.; Ahamad, T.; Zakaria, M. B.; Dou, S. X.; Yamauchi, Y.; Hossain, M. A. Prussian Blue Derived Iron Oxide Nanoparticles Wrapped in Graphene Oxide Sheets for Electrochemical Supercapacitors. *RSC Adv.* **2017**, *7*, 33994-33999.

[17] Sun, S.; Zhai, T.; Liang, C.; Savilov, S. V.; Xia, H. Boosted crystalline/amorphous $Fe_2O_{3-\delta}$ core/shell heterostructure for flexible solid-state pseudocapacitors in large scale. *Nano Energy* **2018**, *45*, 390-397.